

# PERIODICITY ANALYSIS IN THE LIGHT CURVES OF RED GIANT STARS

---

MARCHAND Maxime, 3rd year Bachelor student, University of Geneva  
TRABUCCHI Michele, MOWLAVI Nami, University of Geneva, Department of Astronomy (Supervisors)

## Abstract

This paper reviews the work done in the context of the 3rd year Bachelor Laboratories in the Department of Astrophysics of the University of Geneva. This work concerned the analysis of periodicity in the light curves of stars with mass comparable to that of the Sun as they reach the end of their life. The Color-Magnitude and the Period-Luminosity diagrams have been used to study a set of stars located in the Large and Small Magellanic Clouds. We modeled the Period-Luminosity relations in the Clouds and used them to measure the distance of the SMC relative to the LMC, the result being in agreement with literature values within the errors.

## Contents

<b>1</b>	<b>Introduction</b>	<b>2</b>
<b>2</b>	<b>Theory</b>	<b>2</b>
2.1	Theory and observations . . . . .	2
2.1.1	Apparent and absolute magnitudes, distance modulus . . . . .	2
2.1.2	Black body, spectral energy distribution . . . . .	2
2.1.3	Relation between color and temperature . . . . .	3
2.1.4	Relation between Period and luminosity . . . . .	3
2.1.5	Hertzsprung–Russell diagram (theoretical) and color-magnitude diagram (observed) . . . . .	5
2.2	Stellar evolution . . . . .	5
2.2.1	Before AGB . . . . .	5
2.2.2	During AGB . . . . .	6
2.3	Stellar pulsation . . . . .	7
<b>3</b>	<b>Data</b>	<b>8</b>
3.1	Source of data . . . . .	8
3.2	Color Magnitude diagrams . . . . .	8
<b>4</b>	<b>Methods and analysis</b>	<b>9</b>
4.1	LC processing . . . . .	9
4.2	Analysis of the Period Luminosity relation . . . . .	10
4.3	Derivation of the distance modulus . . . . .	10
<b>5</b>	<b>Results</b>	<b>11</b>
<b>6</b>	<b>Conclusion</b>	<b>12</b>
<b>A</b>	<b>Error estimation for the distance modulus</b>	<b>13</b>

# 1 Introduction

Stars of low mass ( $M \lesssim 8 M_{\odot}$ ) reaching the end of their life, and destined to become white dwarfs, exhibit a periodic behaviour in the emission of light. This behaviour is studied in order to understand physical events occurring within them. In this work, we study this property on a set of stars located in the Large Magellanic Cloud, whose data come from ground-based (OGLE) and space-based (AllWISE, *Gaia*) observation points that measured their luminosity in different parts of the electromagnetic spectrum. We also realize the color-magnitude and period-luminosity diagrams, that are widely used in astrophysics to study the structure and evolution of stars.

# 2 Theory

We summarize here some details about theoretical points and physical quantities that are needed in this work.

## 2.1 Theory and observations

### 2.1.1 Apparent and absolute magnitudes, distance modulus

For historical reasons, the luminosity of stars is measured in magnitudes, based on naked-eye observations. The stars were usually sorted into a system of 6 grades, 1 for the brightest stars, 6 for the faintest. Formally, the magnitudes  $m_1$  and  $m_2$  of two stars are related by :

$$m_2 - m_1 = -2.5 \log_{10} \left( \frac{L_2}{L_1} \right) \quad (1)$$

Eq. (1) allows us to make two comments :

1. Considering  $m_2 > m_1$ , one can see that the magnitude is inverted with respect to the luminosity.
2. The luminosity evolves in a logarithmic way : This is due to the logarithmic response of the human eye.

Observational quantities that are measured must always be considered with precautions. For instance, the *apparent* magnitude of a star located very far from Earth may be altered by obstacles such like the molecules or the dust located around it, or gas clouds located between the star and the observer. In general, the closer a star is, the brightest it appears. We then need a quantity that expresses the magnitude of a star, regardless of its distance, that will allow us to compare the true brightness

of stars and study their physics. This quantity is called *absolute* magnitude, and it corresponds to the brightness of a star, supposing that it is located at a distance of 10 pc from the observer.

Considering a star at distance  $d$ , the flux we receive from it is the ratio of its luminosity to the surface of a sphere of radius  $d$ ,  $f = L/(4\pi d^2)$ . Therefore the relation between apparent and absolute magnitudes (denoted by  $m$  and  $M$ , respectively), is:

$$m - M = -2.5 \log \left[ \left( \frac{10}{d} \right)^2 \right] = 5 \log(d) - 5 \equiv \mu, \quad (2)$$

where  $\mu$  is called *distance modulus* and is also measured in magnitudes.

### 2.1.2 Black body, spectral energy distribution

The black body is a subject of great importance in physics, and also in astronomy for reasons that will be explained later in this report. A black body is an object characterized by the fact that it absorbs every incoming radiation, and returns it in the form of thermal radiation. This emission is described by Planck's law :

$$B_{\lambda}(T) = \frac{2\pi hc^2}{\lambda^5} \frac{1}{e^{hc/k\lambda T} - 1} \quad (3)$$

The spectral energy distribution for different values of the temperature  $T$  is illustrated in Fig. 1. As an other way to understand this law, one can consider the quantity  $B_{\lambda}d\lambda$ , that corresponds to the energy emitted in wavelengths located between  $\lambda$  and  $\lambda + d\lambda$ , per unit surface, per unit time.

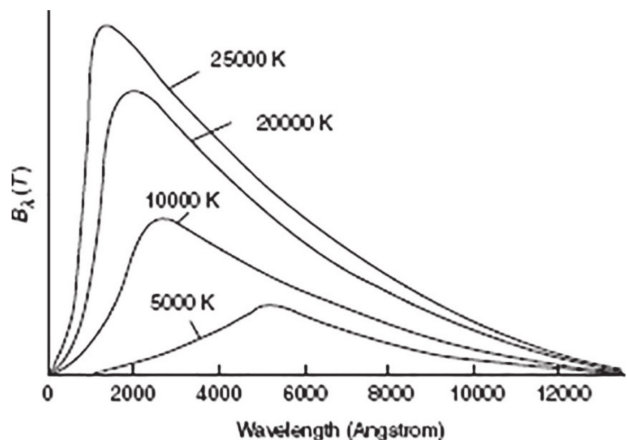


**FIGURE 1:**  $B_{\lambda}(T)$  for different values of the temperature  $T$ . The figure is taken from Cesare BARBIERI and Ivano BERTINI, *Fundamentals of Astronomy* [2].

As we can observe in Fig. 1, the maximum of emission seems to decrease as the temperature increases. This phenomenon is known as Wien's displacement law, connecting the wavelength  $\lambda_0$

where the peak of emission is located with the temperature  $T$  as :

$$\lambda_0 T = b \quad (4)$$

Where  $b$  is a constant.

The importance of the black body in astronomy comes from the fact that the spectral energy distribution of a star seems very close to that of a black body, which allows us to consider them as such, even if it is not true. We will then be able to study their physics using the properties of black bodies.

### 2.1.3 Relation between color and temperature

The temperature at the surface of a star is not a quantity that can be directly measured. Fortunately, we are able to estimate it using indirect methods, for instance when considering the differences in emission of a star in the different wavelength intervals. As we discussed in the previous section, the spectral energy distribution of stars is similar to that of a black body. Thus, because of Wien's displacement law, the peak emission occurs towards short wavelengths in hot stars compared to cool stars. For one star, one can compare observations made with different photometric filters, that isolate light of specific wavelength ranges, or *bands* (as exemplified in Fig. 2). Let us suppose that we have measured the luminosity of a star with two different bands  $\lambda_1$  and  $\lambda_2$ . Using Planck's law, it can be shown that the ratio of the corresponding fluxes  $f_{\lambda_1}$  and  $f_{\lambda_2}$  is a function of its temperature  $T$ . Therefore, through Pogson's law (Eq. 1) the difference between the magnitudes of that star corresponding to those two bands gives information about the stellar temperature:

$$m_{\lambda_1} - m_{\lambda_2} = -2.5 \log \left( \frac{f_{\lambda_1}}{f_{\lambda_2}} \right) = f(T). \quad (5)$$

Such a difference is called *color index* (or simply *color*) of the star. Given two stars, the one having the largest color index is said to be *redder* than the other, because its light emission is shifted towards longer wavelength compared with the other star, that is said to be *bluer*. A relatively red color is an indication of a relatively low temperature.

This approach is based on the assumption that stars are black bodies, which is not exactly true. For this reason, the temperature derived this way is not exactly the same as the temperature at the stellar surface, although it is often close. We call it *effective temperature* ( $T_{\text{eff}}$ ), which is formally defined as the temperature of a hypothetical black body having the same radius and emitting the same amount of radiant energy as the star under consideration.

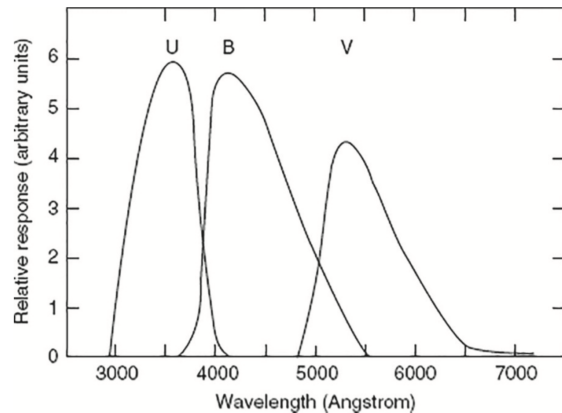


**FIGURE 2:** An example of the response of a UBV filter, allowing observations in the **ultraviolet**, **blue** and **visible** bands. The figure is taken from Cesare BARBIERI and Ivano BERTINI, *Fundamentals of Astronomy* [2].

### 2.1.4 Relation between Period and luminosity

Stars are almost static objects, in which the collapse due to self gravity is balanced by the thermodynamic pressure due to energy released by nuclear reactions occurring near the stellar center. However, given the right physical conditions, their outermost layers can exhibit an oscillating motion, expanding and contracting cyclically. Once this motion is set in place, it is self-excited, as any given contraction causes an energy build-up that will fuel the subsequent expansion. This process, called *stellar pulsation*, occurs for stars approaching the end of their life as the ones studied in this work. When contracting, a star becomes hotter and brighter, while the opposite occurs during expansion, so the pulsation can be observed as a cyclic variation of luminosity. The period  $P$  of this pulsation carries information on the physical structure of a star. In particular, the period of a star is related to its mean density  $\bar{\rho}$ :

$$P \propto \bar{\rho}^{-1/2}. \quad (6)$$

This relation results from the fact that pulsation is a dynamical process, and thus occur over a characteristic time scale. The latter is comparable to the time  $t$  that a test particle would take to get to the center of a star, starting from the surface at a distance  $R$ . Let consider for simplicity that all the mass  $M$  of the star is confined in its center, and that the test particle encounters no effects of viscosity, as illustrated in Fig. 3 :

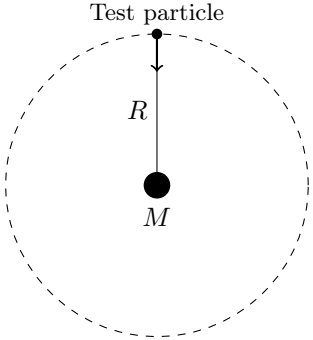


**FIGURE 3:** All the mass  $M$  of the star is confined in the center of it. We let a test particle fall from a distance  $R$  at initial speed  $v_0 = 0$ .

The classical trajectory of the particle is deduced by integration of Newton's second Law :

$$x(t) = x_0 + v_0 t + \frac{1}{2} g t^2 \quad (7)$$

We set the initial conditions to  $x_0 = v_0 = 0$ . The acceleration due to the gravitation is :

$$g = \frac{GM}{R^2} \quad (8)$$

The time needed for the particle to reach the center is then :

$$t = \left( \frac{2R}{g} \right)^{\frac{1}{2}} \quad (9)$$

$$= \left( \frac{2}{G} \right)^{\frac{1}{2}} \left( \frac{R^3}{M} \right)^{\frac{1}{2}} \quad (10)$$

$$= c \cdot \bar{\rho}^{-1/2} \quad (11)$$

A more rigorous derivation of the dynamical time scale (see for instance [4]) gives the same proportionality.

One of the most important physical aspect studied in this work is the fact that one can find a relation between the period and the intrinsic luminosity of a star, or its absolute magnitude. One can find the type of relation by making two observations :

**1** – According to Stefan Boltzmann's law, the luminosity  $L$  of a star is related to its radius  $R$  and effective temperature  $T$  by:

$$L = 4\pi R^2 \sigma T^4. \quad (12)$$

In the case of the Sun, whose properties are denoted  $L_\odot$ ,  $R_\odot$ , and  $T_\odot$ :

$$L_\odot = 4\pi R_\odot^2 \sigma T_\odot^4 \quad (13)$$

Taking the logarithm of the ratio of the two equations above allows us to express Eq. (12) in solar units:

$$\log \left( \frac{L}{L_\odot} \right) = 2 \log \left( \frac{R}{R_\odot} \right) + 4 \log \left( \frac{T}{T_\odot} \right) \quad (14)$$

**2** – The luminosity of a star is correlated to its mass, for reasons that we will detail after. For the moment, let us assume that the mass  $M$  is proportional to a certain power  $a$  of the luminosity  $L$ . One can write :

$$M \propto L^a \Rightarrow \log \left( \frac{M}{M_\odot} \right) = a \log \left( \frac{L}{L_\odot} \right) \quad (15)$$

Knowing that the period  $P$  is proportionnal to the mean value of the density  $\bar{\rho} = \frac{M}{V} = \frac{M}{\frac{4}{3}\pi R^3}$ , one finds that the period evolves like :

$$P \propto M^{-\frac{1}{2}} R^{\frac{3}{2}} \propto \left( \frac{M}{M_\odot} \right)^{-\frac{1}{2}} \left( \frac{R}{R_\odot} \right)^{\frac{3}{2}} \quad (16)$$

Taking the logarithm :

$$\log(P) = -\frac{1}{2} \log \left( \frac{M}{M_\odot} \right) + \frac{3}{2} \log \left( \frac{R}{R_\odot} \right) + \text{const} \quad (17)$$

Inserting eq (14), one gets :

$$\begin{aligned} \log(P) &= -\frac{1}{2} \log \left( \frac{M}{M_\odot} \right) + \frac{3}{4} \log \left( \frac{L}{L_\odot} \right) \\ &\quad - 3 \log \left( \frac{T}{T_\odot} \right) + \text{const} \end{aligned} \quad (18)$$

Using eq (15), one finally finds :

$$\log(P) = \gamma + \delta \log \left( \frac{L}{L_\odot} \right) \quad (19)$$

Where the term  $\log(T/T_\odot)$  has been put in the constant  $\gamma$  because in many cases it is negligible compared with the luminosity term. This relation has a crucial importance as it can be used to determine stellar distances. Indeed, if the apparent magnitude of a star is known and its period is measured, the absolute magnitude can be derived from the period and can be used to compute the distance modulus. An other important aspect considering Eq. (18) is that it connects the mass of a star with its intrinsic luminosity. It can be understood by considering a very massive star, whose high internal pressure will allow its core to reach much higher temperatures, resulting in a more efficient nuclear activity. This process will create more energy, allowing the star to be brighter.

### 2.1.5 Hertzsprung–Russell diagram (theoretical) and color-magnitude diagram (observed)

One of the most important diagnostic tools in stellar astrophysics is the Hertzsprung–Russell diagram (HRD). Variables describing stars like the luminosity, or the temperature can be associated on a diagram, that gives us precious information about the evolutionary state of them. A version of such a diagram is shown in Fig. 4. This graph illustrates the absolute luminosity with respect to the temperature. The HRD is characterized by a long diagonal section, named the *Main Sequence*. It is usually the densest part of the diagram, because it represents the longest period of the evolution of a star, when it burns hydrogen in its core. Points located above the diagonal corresponds to the red giants, and points below represents the white dwarfs.

As we discussed in the previous section, the effective temperature of a star is not easy to derive but is related to its color index. Then, one can build an “observational” HR diagram based on the color and the magnitude, that is, a color-magnitude diagram (CMD). Fig. 5 shows an example of such a diagram for a set of stars coming from the HIPPARCOS catalog.

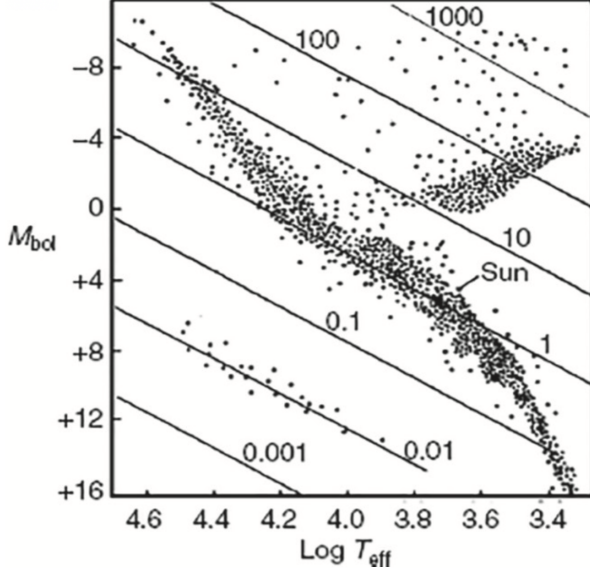


**FIGURE 4:** An example of Hertzsprung–Russell diagram. One recognizes the large diagonal from top left to bottom right as the main sequence. The figure is taken from Cesare BARBIERI and Ivano BERTINI, *Fundamentals of Astronomy* [2].

Using the color-magnitude diagram on a set of stars is very useful to determine the average age of it, as one can observe how many stars remains on the main sequence, and whether they move below or above the diagonal.

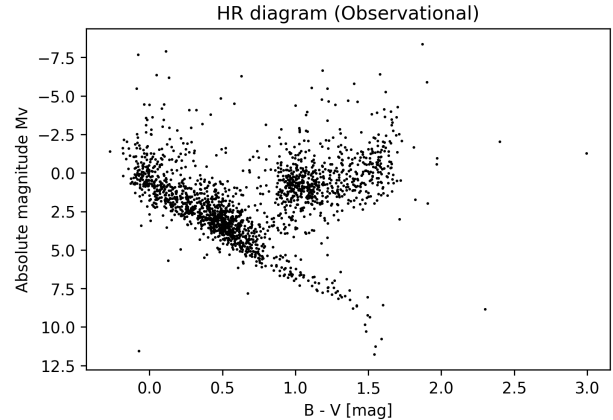


**FIGURE 5:** Observational diagram of stars coming from the HIPPARCOS catalog.

## 2.2 Stellar evolution

We summarize here the main steps occurring during the life of a star. This part is based on the book *Pulsating Stars* by CATELAN and SMITH [3]. The stars studied in this work are in the Asymptotic Giant Branch (AGB) evolutionary phase, approaching the end of their lives. Therefore, we split our summary of stellar evolution in two parts: before and during the AGB.

The predominant factor that determines the evolution of a star is its mass. We are interested here in the evolution of low-mass ( $0.8M_{\odot} \lesssim M \lesssim 2.5M_{\odot}$ ) and intermediate-mass ( $2.5M_{\odot} \lesssim M \lesssim 8M_{\odot}$ ) stars. One can illustrate the life of a star thanks to a theoretical HR diagram, that allows us to observe the changes in luminosity and temperature of it. An example of a low-mass star evolution is shown in Fig. 6.

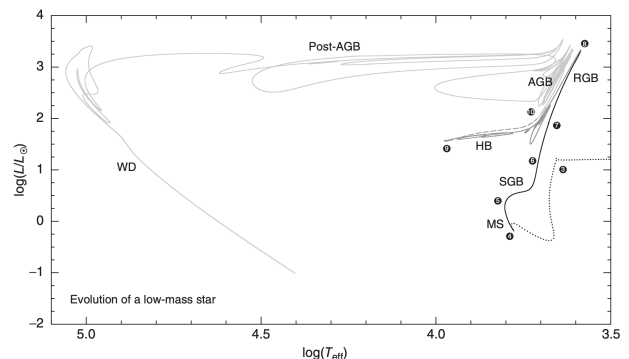


**FIGURE 6:** Evolution of a low-mass star, resulting from a numerical simulation. This figure is taken from the book *Pulsating Stars* by CATELAN and SMITH [3].

### 2.2.1 Before AGB

The matter of which a star is made comes from large gas clouds, after having collapsed due to the gravitational force. Indeed, as the mass of the clouds evolves with respect to the radius  $r$  like  $r^3$ , the force

due to the gravitation evolves like  $r^{-2}$ . This difference in behaviour with respect to the size must induce an instability in the system. Astronomer James JEANS deduced a critical length  $\lambda_J$ , above which a cloud begins to collapse.

A hydrogen core that gently begins to heat up is formed while matter continues to accumulate. After some time, the star will have reached its final mass. The star is born once the energy release from central nuclear reactions becomes able to balance gravitational collapse. The star burns hydrogen into helium according to the PP chain (or the CNO cycle if the mass is large enough). Stars that are burning hydrogen in their core are located on the Main Sequence of the HRD, where they spend most of their life. The stellar structure is illustrated on the first diagram of Fig. 7.

When all hydrogen is consumed in the core, nuclear reactions stop and the stellar core now made of helium resumes contracting under the effect of gravity. The temperature on the edge of the helium core is high enough for hydrogen, still present there, to fuse into helium, powering the star. While the core keeps contracting, the stellar layers outside the *nuclear shell* where hydrogen is burnt expand to a large size and cool down. The star has begun his ascention on the Red Giant Branch (RGB in Fig. 6). During this process, the structure of the star consists of a helium core, wrapped in a thick shell composed of hydrogen transforming to helium, as illustrated on the second diagram of Fig. 7. The Helium core increases, as the hydrogen shell reduces in thickness. After a critical point, the helium core reaches the *Schönberg-Chandrasekhar mass*, which is the maximum mass allowed for the helium core before it can no longer support the hydrogen layer. At this point the star has reached the end of the RGB.

Because of the self-gravity, the core consists of an electron-degenerate gas. At this point the behaviour of the star is different between low-mass and intermediate-mass stars. Concerning intermediate-mass stars, the degeneracy is cancelled before the temperature becomes high enough to allow the fusion of helium into carbon. The pressure in the core increases in response to the heating caused by the ignition of helium fusion, so that the core expands preventing an uncontrolled increase in temperature. This process will allow the fusion of helium to begin progressively.

Concerning low-mass stars, the fusion of helium begins as the core is still electron-degenerate. Due to the fact that the pressure is not dependent on the temperature in a electron-degenerate gas, the helium burning process will not be regulated by the pressure, generating a non-controlled chain reaction. Indeed, as the temperature of the core increases, more helium atoms will be able to fuse into carbon, generating more heat, etc. This process is called *Helium flash*,

because the total energy generated by this process is so high that the luminosity of the core can be comparable as the one of an entire galaxy.

Whether or not the Helium flash occurs, a star then settles in a stage of quiet core-helium burning. The envelope has contracted significantly compared with the RGB phase, and the star tends to appear fainter and hotter in the HRD (corresponding to the horizontal branch (HB) part in Fig. 6). The structure of the star at this point of its evolution is illustrated on the third diagram of Fig. 7. Once helium is exhausted in the core, the star will begin its ascension in the Asymptotic Giant Branch, named so because it appears parallel to, and converging with, the RGB in the HRD.

### 2.2.2 During AGB

The structure of a star while beginning its ascension on the AGB consists of a C/O core, surrounded by a He-burning shell, a H-burning shell, and a convective envelope, as illustrated in the fourth diagram of Fig. 7.

The reactions occurring in the helium shell are unstable. At frequent time intervals ( $\sim 10^4 - 10^5$  years, depending on the stellar mass), the shell undergo a thermonuclear runaway. This event temporarily shuts down the nuclear reactions in the shells. This phenomenons are what is called *thermal pulses*. During the period of time when the nuclear reactions aren't occurring, the convective envelope is able to reach the inner regions of the star, resulting in the transport of the nucleosynthesis on the surface of it. This process is called *3rd dredge up*. Among the molecules brought to the surface, one finds carbon, and depending on whether the amount of carbon molecules is sufficient, the 3rd dredge up may be able to transform a star rich in oxygen, namely a O-rich, into a C-rich star. This difference in the chemical composition has already an impact on the photometric properties of the star, as we will see in Sec. 3.2.

For AGB stars, the temperature is cool enough to increase the tendency of oxygen and carbon to form carbon monoxide (CO molecules). The remaining molecules will then join together to form TiO, VO, H<sub>2</sub>O, etc. for O-rich stars, and C<sub>2</sub>, CN, HCN, etc. for C-rich stars. This will also introduce differences in the photometric properties of both types of stars. As it will be explained more in details in Sec. 2.3, AGB stars undergo stellar pulsation, and the more a star is evolved on the AGB, the more the amplitude of oscillation will increase. When it becomes large enough, this process is able to drive shock waves in the atmosphere, compressing the star. This results in an increase of the density and a decrease in temperature, and will favor the formation of dust grains.

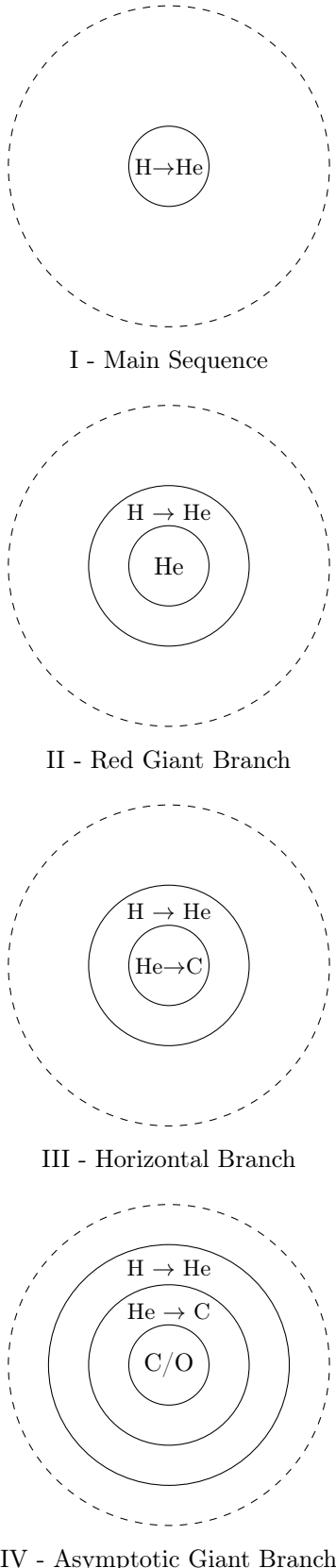


**FIGURE 7:** Evolution of the structure of a star of low or intermediate mass during the different types of nuclear burnings it experiences during its life.

At this point the star will seem to me much fainter as it is actually. This is due to the high capacity of dust to absorb the stellar radiation in visual wavelengths. Because of this absorption, momentum is transferred to the grains, that move away from the star, dragging gas with them. This process, namely *stellar wind* induces a loss of mass of the star.

As the mass decreases, the star progressively loses its envelope, preventing the pressure to be high enough to allow the star to continue its nuclear reactions. This marks the death of the star, leaving a white dwarf.

### 2.3 Stellar pulsation

As briefly discussed in Sec. 2.1.4, the physical processes occurring in the stars, namely the balance between the collapse due to self gravity and the thermodynamic pressure generated by the nuclear reactions in the stellar center, can be perturbed resulting in an oscillatory motion of the outermost layers of the star. Naturally, this phenomenon has an impact on the light emission of the star as it causes its temperature to vary, and so its spectral energy distribution. Depending on the properties of their light curves one classifies AGB variable stars in three main categories, namely Miras, Semi Regular Variables (SRVs) and OGLE Small Amplitude Red Giants (OSARGs). The differences occurs in the differences in magnitudes in the oscillations (peak to peak luminosities). As Miras have the largest differences in amplitude, OSARGs have the smallest ones.

As any physical system, and provided the good conditions, the oscillating motion of a star can appear in an infinite number of modes of oscillation, or natural frequencies of resonance (See for instance Melde's experiment). We speak then of a fundamental mode, having the longest period (or smallest frequency), and zero radial nodes, and its overtones. The first one has one radial node and a smaller period than the fundamental mode, and so on for the higher overtones.

The number of overtones in which a star can oscillate highly depends on its structure. In general, relatively compact stars will oscillate in many high-order modes while more expanded, less dense stars pulsate in a small number of low-order modes (as it is the case during their ascension on the AGB). As an illustration, Fig. 8 illustrates the light curves of stars of each type. In the context of this work, the analysis of periodicity of the AGB stars won't exceed 3 periods.

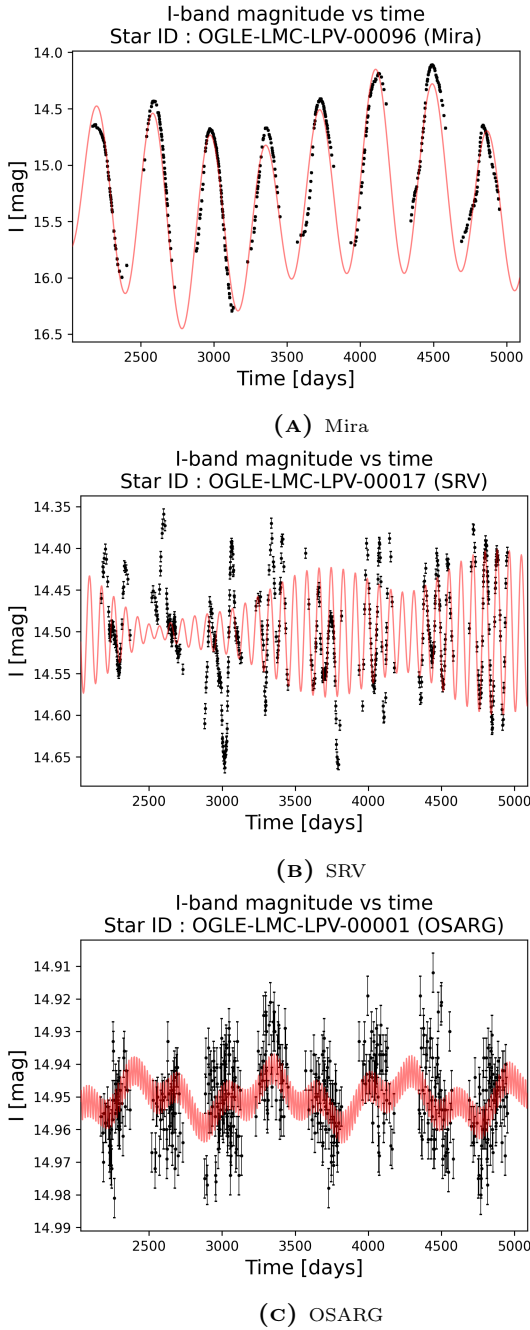


**FIGURE 8:** Light curves of the stars (from top to bottom: a Mira, a SRV, and a OSARG) obtained by OGLE. More details about the realization of these figures can be found in Sec. 4.1 and in description of Fig. 11.

### 3 Data

In this section, we present the data that has been used in order to analyze the AGB stars.

#### 3.1 Source of data

The main data used in this report comes from the Optical Gravitational Lensing Experiment (OGLE) [8, 1] and the Two-Micron All-Sky Survey (2MASS)

[7]. The OGLE project observes the sky with a telescope based in Chile. We are interested here in the Large Magellanic Cloud (LMC) and the Small Magellanic Cloud (SMC), two satellite galaxies of our own Galaxy, the Milky Way. Fig. 9 shows the sky coverage of OGLE on these two galaxies.

OGLE provides us with processed data, as the periods, the amplitudes and mean magnitudes in the  $V$  ( $\sim 0.55\mu\text{m}$ ) and  $I$  ( $\sim 0.9\mu\text{m}$ ) bands. It also provides the light curves of each stars, that consist of  $I$ -band magnitudes as a function of time. 2MASS provides the magnitudes in the  $J$  ( $\sim 1.25\mu\text{m}$ ) and  $K_s$  ( $\sim 2.17\mu\text{m}$ ) bands.

We have thus data covering the visual range of the electromagnetic spectrum thanks to OGLE, and covering the near-infrared thanks to 2MASS. This will be very convenient since the stars concerned in this work have a major emission in the infra-red range, while their variability is most easily observed in the visual range. The cross match between these two data sets and *Gaia* EDR3 [6] will give us enough information to study this set of stars.

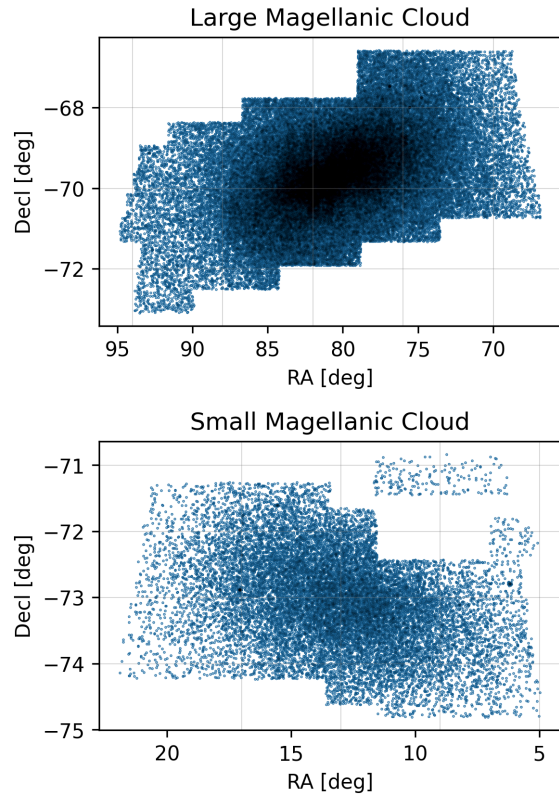


**FIGURE 9:** Sky coverage of OGLE for the LMC (top) and SMC (bottom).

#### 3.2 Color Magnitude diagrams

Before discussing the processing of the light curves, we briefly examine the distribution of the adopted sample in the optical and near-infrared color-magnitude diagrams (CMDs).

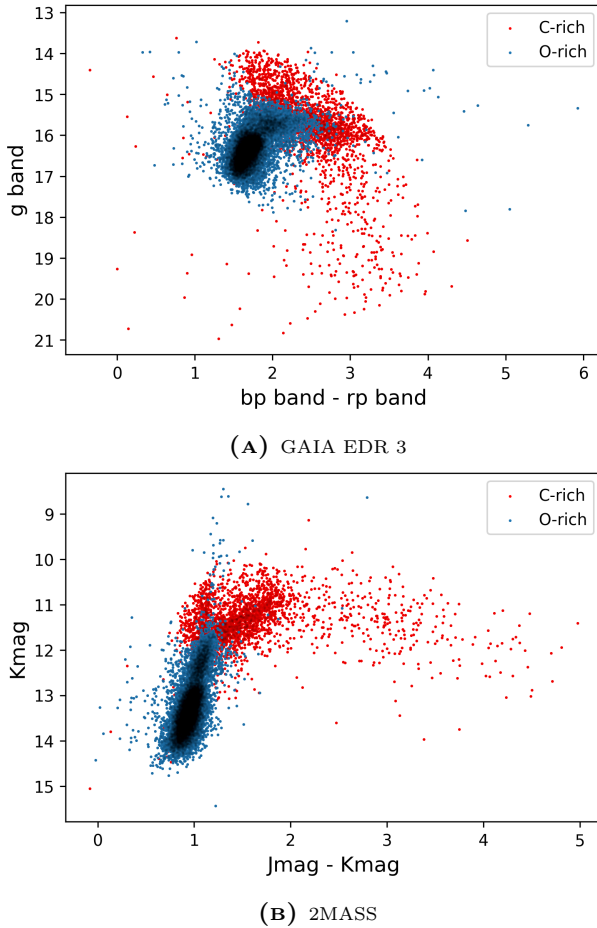


**FIGURE 10:** Color Magnitude diagrams for stars located in the SMC. Red dots correspond to C-rich stars, and blue dots to O-rich stars. Fig. (a) is made with observations using photometric filters in the visible band. Fig. (b) is made with observations made in the infrared band. The data used to realize these CMDs come from OGLE, *Gaia* and 2MASS.

Fig. 10 represents the color-magnitude diagrams for the LPVs in the SMC observed by OGLE, one using photometric data from the *Gaia* database, the other from the 2MASS database. One recalls that, as *Gaia* measured the luminosity in the visible part of the spectrum, 2MASS measured it more in the infrared. We make the distinction between O-rich and C-rich stars (based on the classification provided in the OGLE catalog). Such a difference in the chemical composition of the star is due to the *3rd dredge up* and has non negligible impacts on the photometric properties of the star, as we can observe on the CMDs presented above. Fig. 10a is the CMD in the visible band. One clearly observes that the C-rich stars tend to be displaced on the diagram. This is due to the fact that the carbon molecules present on the surface of the star absorbs some of the light emission of the stars, making them appear colder and fainter.

Concerning Fig. 10b, in the infra-red band, the most evolved stars also seems to appear redder and fainter.

This is also due to the absorption of the light by C molecules.

This tendency appearing in the two CMDs can be further explained, thanks to the theoretical points discussed in the previous sections. Since the stars are cold, the molecules are more able to cluster together, resulting in the formation of dust around them. This makes the stars appear redder and fainter.

The presence of dust around the star has a crucial impact on the evolution of it. Indeed, while blocking the light emission of the star, the dust absorbs the photons emitted. Energy is transferred to it, and the dust is then pushed away for the star, resulting in the loss of mass of it. This phenomenon is what is called *stellar winds*. As the external envelope is gradually removed from the star, the pressure is not strong enough to keep the star warm, preventing it to continue the thermonuclear reactions in its core. The star is compelled to die.

## 4 Methods and analysis

### 4.1 LC processing

At first, the light curves will be processed to extract the three main periods. For this purpose we will use the Lomb-Scargle algorithm (LSA), a tool widely used in astronomy. More details about the LSA can be found in the article from VANDERPLAS, *Understanding the Lomb-Scargle Periodogram* [9]. Its use is the same as a Fourier analysis, except it allows us to analyze the periodic behaviour of a sequence of measurements that are not regularly distributed in time (as it is often the case with astrophysical observations).

For a given sequence, the LSA constructs a *periodogram*  $LS(P)$ , indicating for each period  $P$  how well a cosine curve with that period fits the data. A periodogram having a net distinguishable maximum at  $P = P_0$  indicates that the signal observed has a period most likely similar to  $P_0$ .

The implementation of the analysis will return us the best fit parameters, namely the amplitude  $A$ , the phase offset  $\phi$  and the magnitude offset  $m_0$ . These values allow us to construct the best cosine model  $f(t) = A \cos(2\pi t/P + \phi) + m_0$  of the light curve.

However, the exactness of this model will rarely, if ever be perfect. The difference between the model and the observations is called the *residual*. In this work, we will apply the LSA on the light curves concerning stars having not only one, but multiple periods. In this case the residual will necessarily not be zero, due to the presence of these other periods. To solve this problem, we will iterate the LSA on the residuals, that will be obtained by subtracting at each iteration the model of the previous period. This procedure will compute the best fit parameters  $A_1$ ,  $\phi_1$  for the first

period  $P_1$ ,  $A_2$ ,  $\phi_2$  for the second period  $P_2$ , etc. We will then be able to construct the best fit model, which consists of the sum of the three models of each periods :

$$\begin{aligned} f(t) = m_0 &+ A_1 \cos(2\pi t/P_1 + \phi_1) \\ &+ A_2 \cos(2\pi t/P_2 + \phi_2) \quad (20) \\ &+ A_3 \cos(2\pi t/P_3 + \phi_3) \end{aligned}$$

Fig. 11 illustrates the analysis made on one of the stars.

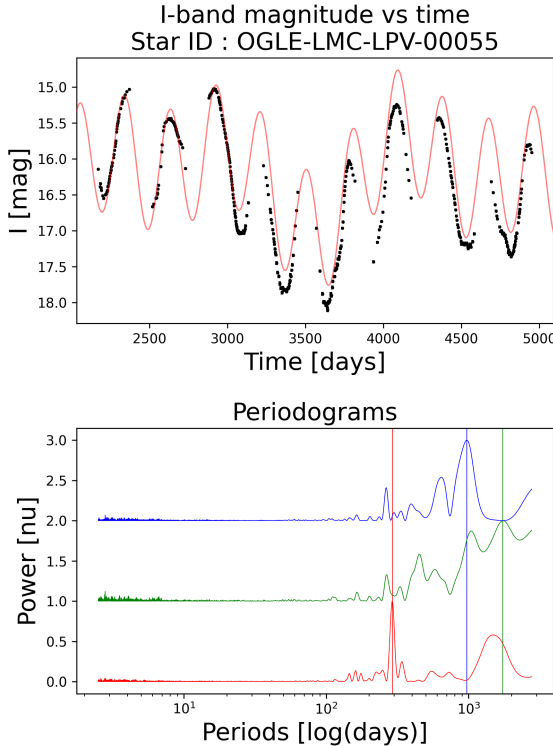


**FIGURE 11:** (Above) The black points represent the observed light curve of the star obtained by OGLE. The red curve represents the mathematical model (corresponding to the sum of the three models related to each period). (Below) The LS periodograms of the observed light curve (red) and after subtracting the model with one and two periods (green and blue, respectively). The periodograms are normalized to their maximum and offset with respect to each other by an arbitrary amount. The three vertical lines localize the three first periods, obtained after iterating the LSA, as explained in the paragraph.

## 4.2 Analysis of the Period Luminosity relation

To analyze the period-luminosity relation, we choose a set of 600 stars, containing 300 Miras and 300 SRVs. This set will contain enough stars to obtain a precise value for the linear regression. We then plot the period-luminosity diagram (PLD). The  $J$  and  $K_s$  bands from 2MASS are used. In fact, we build a new quantity

$$W_{J,K_s} = K_s - 0.686 \cdot (J - K_s) \quad (21)$$

that helps correcting for the fact that some stars are surrounded by dust and thus appear fainter. We then plot the magnitude with respect to the logarithm of the first period, as shown in Fig. 13. According to equation (19), we should get a linear relation, while multiple such relations appear in the diagram. This happens because the primary period (the first one we detected with our method) does not necessarily corresponds to the fundamental mode, that we are interested in analyzing. By comparison with the results of [10], we identify the central relation in our PLD with the fundamental mode (between the black lines in Fig. 13), and exclude all other periods. For stars whose primary period is excluded this way, we consider the possibility that the secondary or tertiary period is actually associated with the fundamental mode. We check its position in the PLD and, if it is located in the central relation, we adopt it in place of the primary period. After this procedure, we are left with a sample of 523 stars; 294 are Miras, while 229 are SRVs. For the remaining 77, we could not measure the fundamental mode period. We are then able to get the  $\gamma$  and  $\delta$  coefficients in eq. (19) by fitting a linear functional form to the distribution in the diagram. These will be used to determine the distance modulus for the SMC, that will be discussed in the next section.

## 4.3 Derivation of the distance modulus

We are now able to derive the distance modulus of the SMC. As a reference, we use the values from Richard DE GRIJS et al., *Toward an Internally Consistent Astronomical Distance Scale* [5] :

$$\mu_{\text{LMC, ref}} = 18.49 \pm 0.09 \text{ mag} \quad (22)$$

$$\mu_{\text{SMC, ref}} = 18.96 \pm 0.02 \text{ mag} \quad (23)$$

We want to derive an alternative estimate of  $\mu_{\text{SMC}}$ . Due to the different distances, the linear relation between the logarithm of the period and the luminosity,

$$W_{J,K_s} = m \log(P) + q \quad (24)$$

will be offset by a value  $\delta q$ , as illustrated in Fig. 12. We assume that the difference in the distance modulus  $\delta \mu$  is equal to the shift of the linear regression  $\delta q$  :

$$\delta \mu = \mu_{\text{LMC}} - \mu_{\text{SMC}} = \delta q \quad (25)$$

This means that we assume that the slope of the relation is the same in the LMC and SMC, which is approximately true. Knowing  $\mu_{\text{LMC, ref}}$ , we can then write :

$$\mu_{\text{SMC}} = \mu_{\text{LMC}} - \delta q \quad (26)$$

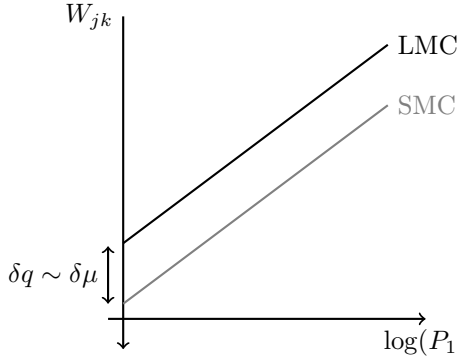


**FIGURE 12:** The linear relation is shifted due to the distance.

## 5 Results

We now present the linear relation computed on the Period Luminosity diagrams, and the estimation of the distance modulus of the SMC according to the method described in Sec. 4.3.

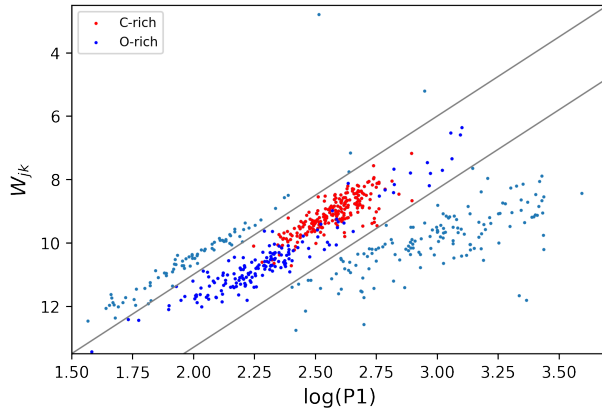


**FIGURE 13:** Period luminosity relation for the stars in the LMC.

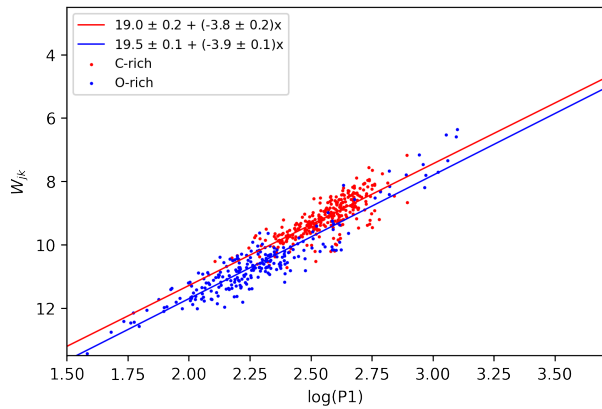


**FIGURE 14:** Linear regressions for the stars in the LMC.

Fig. 13 represents the period luminosity relation (PLR) for the set of stars located in the LMC. The points between the two gray separation lines represent periods attributed to pulsation in the fundamental mode. The other points are excluded from our analysis. We also made the distinction between C-rich and O-rich stars. We then make the linear regression for both data sets. The results are shown in Fig. 14. For an expression in the form of Eq. (24), one finds :

	$q_{\text{LMC}}$	$m_{\text{LMC}}$
C-rich	$19.0 \pm 0.2$	$-3.8 \pm 0.2$
O-rich	$19.5 \pm 0.1$	$-3.9 \pm 0.1$

The same procedure is applied to the set of stars located in the Small Magellanic Cloud :

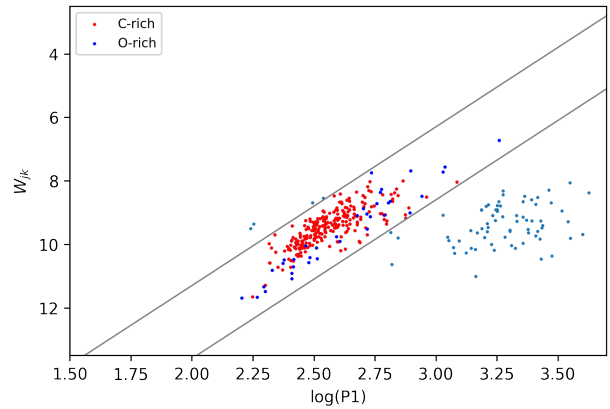


**FIGURE 15:** Period luminosity relation for stars in the SMC.

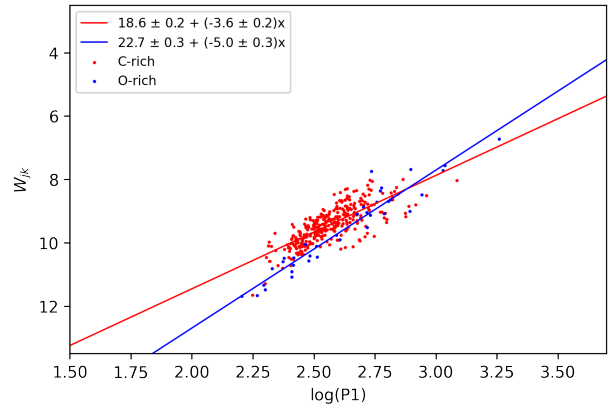


**FIGURE 16:** Linear regressions for the stars in the SMC.

For an expression in the form of Eq. 24, one finds :

	$q_{\text{SMC}}$	$m_{\text{SMC}}$
C-rich	$18.6 \pm 0.2$	$-3.6 \pm 0.2$
O-rich	$22.7 \pm 0.3$	$-5.0 \pm 0.3$

As we can observe in Fig. 16, the slope of the O-rich stars differs from the C-rich stars. This is mainly due to the difference of distribution between the two types of stars (the percentage of C-rich stars is larger in the SMC), and also due to their different photometric properties.

Regarding only the O-rich stars, we can also remark that the slope of the stars in the SMC differ a little bit from the slope of the ones in the LMC. To avoid this problem, we assume for simplicity that the two slopes should be the same, and we compute the linear regression for the SMC setting the slope with the one found for the LMC :

$$f(x) = m_{\text{LMC}} x + q \quad (27)$$

We will then find a more accurate value for  $q$ . Fig. 17 shows the final regression for the O-rich stars in the SMC.

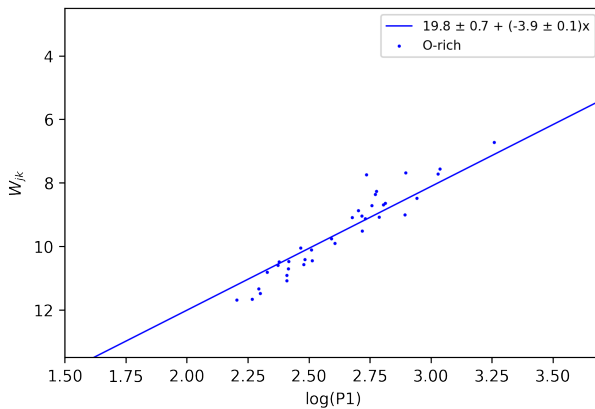


**FIGURE 17:** Regression on the O-rich stars of the SMC, adjusted with the model of the LMC.

We find a value of  $b_{\text{SMC}} = 19.8 \pm 0.7$ . We are now able to compute the distance modulus for the SMC, using equation (26) and the previous results. One gets :

$$\begin{aligned} \mu_{\text{SMC, obs}} &= \mu_{\text{LMC, ref}} - \delta q \\ &= \mu_{\text{LMC, ref}} - (q_{\text{LMC}} - q_{\text{SMC}}) \\ &= 18.8 \pm 0.3 \text{ mag} \end{aligned}$$

Let recall the values for  $\mu$  :

$$\mu_{\text{SMC, ref}} = 18.96 \pm 0.02 \text{ mag} \quad (28)$$

$$\mu_{\text{SMC, obs}} = 18.8 \pm 0.3 \text{ mag} \quad (29)$$

As we can see this result is close to the reference value for the distance modulus. This value has been reached with a relatively small set of stars, which explains the relatively large uncertainty compared with the reference value. The details about the estimation of the error can be found in appendix A.

## 6 Conclusion

The light curves provided by OGLE allowed us to study some properties of low-mass and intermediate-mass stars located in the LMC and the SMC, reaching the end of their life. Thanks to the Lomb-Scargle algorithm, we analyzed the periodicity of the light curves, allowing us to realize their best fit model. Thanks to the observations in different photometric bands from the missions *Gaia* EDR3, AllWise and 2MASS, we realized the color magnitude diagrams of stars located in the SMC and were able to analyze their photometric properties, considering both C-rich and O-rich stars. The investigation of the relation between the period with respect to the luminosity allowed us to estimate the distance modulus of the SMC, obtaining some results relatively close to the reference value taken from the work of Richard DE GRIJS et al. [5]. This work introduced some fundamental notions and commonly used tools in astrophysics, about the evolution of the stars and the periodic behaviour of their luminosity.

## References

- [1] OGLE website <http://ogle.astrouw.edu.pl/>.
- [2] C. Barbieri and I. Bertini. *Fundamentals of astronomy*. CRC Press, Boca Raton London New York, second edition edition, 2021.
- [3] M. Catelan and H. A. Smith. *Pulsating Stars*. 2015.
- [4] J. P. Cox. *Theory of stellar pulsation*. Princeton University Press, 1980.
- [5] R. de Grijs, F. Courbin, C. E. Martínez-Vázquez, M. Monelli, M. Oguri, and S. H. Suyu. Toward an Internally Consistent Astronomical Distance Scale. *Space Science Reviews*, 212(3-4):1743–1785, Nov. 2017.
- [6] Gaia Collaboration, A. G. A. Brown, A. Vallenari, and P. et al. Gaia Early Data Release 3. Summary of the contents and survey properties. *Astronomy and Astrophysics*, 649:A1, May 2021.
- [7] M. F. Skrutskie, R. M. Cutri, R. Stiening, M. D. Weinberg, S. Schneider, J. M. Carpenter, C. Beichman, R. Capps, T. Chester, J. Elias, J. Huchra, J. Liebert, C. Lonsdale, D. G. Monet, S. Price, P. Seitzer, T. Jarrett, J. D. Kirkpatrick, J. E. Gizis, E. Howard, T. Evans, J. Fowler, L. Fullmer, R. Hurt, R. Light, E. L. Kopan, K. A. Marsh, H. L. McCallon, R. Tam, S. Van Dyk, and S. Wheelock. The Two Micron All Sky Survey (2MASS). *Astronomical Journal*, 131(2):1163–1183, Feb. 2006.
- [8] I. Soszyński, A. Udalski, M. K. Szymański, M. Kubiak, G. Pietrzyński, Ł. Wyrzykowski, O. Szewczyk, K. Ulaczyk, and R. Poleski. The Optical Gravitational Lensing Experiment. The OGLE-III Catalog of Variable Stars. IV. Long-Period Variables in the Large Magellanic Cloud. *Acta Astronomica*, 59(3):239–253, Sept. 2009.
- [9] J. T. VanderPlas. Understanding the Lomb–Scargle Periodogram. *The Astrophysical Journal Supplement Series*, 236(1):16, May 2018.

- [10] P. R. Wood. The pulsation modes, masses and evolution of luminous red giants. *Monthly Notices of the Royal Astronomical Society*, 448(4):3829–3843, Apr. 2015.

Figures without any indication of the source were self-made.

## A Error estimation for the distance modulus

We use the formula

$$\Delta f(x_1, \dots, x_n) = \sqrt{\sum_{i=1}^n \left( \frac{\partial f(x_1, \dots, x_n)}{\partial x_i} \Delta x_i \right)^2} \quad (30)$$

In our case :

$$f \equiv \mu_{\text{SMC, obs}} = \mu_{\text{LMC, ref}} - (q_{\text{LMC}} - q_{\text{SMC}}) \quad (31)$$

Computing the partial derivatives leads us to :

$$\frac{\partial \mu_{\text{SMC, obs}}}{\partial q_{\text{SMC}}} = \frac{\partial \mu_{\text{SMC, obs}}}{\partial \mu_{\text{LMC, ref}}} = 1 \quad (32)$$

$$\frac{\partial \mu_{\text{SMC, obs}}}{\partial q_{\text{LMC}}} = -1 \quad (33)$$

Inserting in eq. (30) :

$$\Delta \mu_{\text{SMC, obs}} = \sqrt{\Delta q_{\text{SMC}}^2 + \Delta q_{\text{LMC}}^2 + \Delta \mu_{\text{LMC, ref}}^2} \quad (34)$$

A numerical application leads us to :

$$\Delta \mu_{\text{SMC, obs}} \simeq 0.3 \text{ mag} \quad (35)$$